ACS APPLIED MATERIALS & INTERFACES

Research Article

www.acsami.org

Facile Deposition of YSZ-Inverse Photonic Glass Films

Jefferson J. do Rosário,[†] Pavel N. Dyachenko,[‡] Roman Kubrin,[†] Robert M. Pasquarelli,[†] Alexander Yu. Petrov,[‡] Manfred Eich,[‡] and Gerold A. Schneider*,[†]

[†]Institute of Advanced Ceramics, Hamburg University of Technology, Denickestrasse 15, 21073 Hamburg, Germany

[‡]Institute of Optical and Electronic Materials, Hamburg University of Technology, Eissendorfer Strasse 38, 21073 Hamburg, Germany

Supporting Information

ABSTRACT: An alternative all-colloidal and single-step deposition method of yttrium-stabilized zirconia (YSZ)-infiltrated polymeric photonic glass films is presented. Heterocoagulation of oppositely charged polystyrene (PS) microspheres and YSZ nanocrystals in aqueous dispersions created PS/YSZ core−shell spheres. These composite particles were deposited on glass substrates by a simple drop-coating process. Heterocoagulation impaired self-assembly of the particles, resulting in a disordered structure. Burn-out of the polymer yielded a random array of YSZ shells. The effect of the filling fraction of YSZ between these shells was explored. YSZ-inverse photonic glass films with a thickness below 40 μm achieved 70% reflectance of the incident radiation over a broad wavelength range between 0.4 and 2.2 μm. The YSZ structures demonstrated structural stability up to 1000 °C and maintained high reflectance up to 1200 °C for several hours, thus enabling applications as broadband reflectors at elevated temperatures.

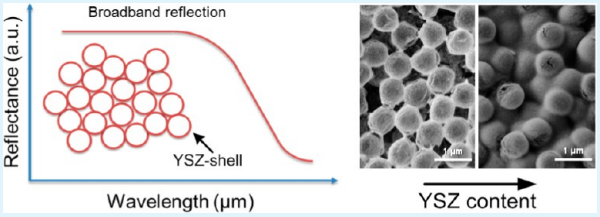

KEYWORDS: *photonic glass, yttrium-stabilized zirconia (YSZ), high-temperature photonics, broadband reflector, thermal barrier coating (TBC), heterocoagulation*

1. INTRODUCTION

The architecture of porous materials has been widely studied for many decades; however, structures on different scales and for new applications are in constant development. In the field of photonics, photonic crystals are well-known ordered structures that affect the propagation of electromagnetic radiation by the presence of a photonic band gap. Disorder has been treated as a disadvantage present in ordered photonic structures due to the multiple scattering promoted. However, scattering is not always detrimental. In recent years, there has been an increasing interest in disordered structures and how light transport behavior in these materials can be beneficial.[1,2]

In 2007, García et al.[3] presented a novel three-dimensional disordered porous material with interesting photonic behavior, the photonic glass. Photonic glasses, a subset of macroporous materials, are formed by a disordered array of monodisperse spheres or pores, referred to as direct or inverted structures, respectively. They can be produced by promoting colloidal instability in a suspension containing polymeric microspheres to deposit a disordered array.[3] Colloidal instability is the key for depositing disordered arrays of monodispered microspheres. Disorder can also be achieved by controlling particle−substrate interactions[4,5] and modifying the solvent,[6,7] e.g., mixtures of water and ethanol. Alternatively, a tailored assembly of colloidal particles in a glass cell was proposed to control the transition between photonic crystals and glasses.[8] Applications such as random lasing,[3,9,10] resonance-dependent Anderson localization,[3,9] and in dye-sensitized photoelectrochemical cells[11] have been suggested. However, the strong scattering of light in the disordered structure and resulting high diffuse reflectance over a broad wavelength range also make photonic glasses highly suitable for broadband reflectors, as can be observed in this study. Broadband reflectors have applications as optical filters,[12,13] high-efficiency omnidirectional reflectors,[12−16] and thermal barrier coatings.[17,18]

Refractory photonic glasses can be used as next-generation thermal barrier coatings (TBCs) in gas turbines that would not only reduce heat transfer by thermal conduction but also effectively reflect thermal radiation. The radiative contribution becomes increasingly significant as the gas inlet temperature of a gas turbine increases.[19] The concept of reflecting TBCs based on multistack photonic crystals was presented recently by Lee et al.[17] Simulations performed in this work have shown that the full coverage of the blackbody radiation spectrum in the relevant temperature range may require up to 10 stacks of inverse opals with different lattice constants because the reflection bands of photonic crystals with a single pore size are rather narrow. Photonic glasses are more suitable for broadband reflectors than multistack photonic crystals. Disordered structures offer the advantage of broadband reflectance which could eliminate the need for depositing multilayer coatings, and their photonic performance is virtually

Received: April 7, 2014
Accepted: July 18, 2014
Published: July 18, 2014

insensitive to structural flaws. At the same time, such disordered structures as well as the ordered ones offer the potential of very low phononic heat conduction: in the case of inverted structures, this is due to their high porosity, and in the case of direct structures this property is a consequence of the limited contact areas between single spheres. Therefore, it is anticipated that the technical feasibility of thermal radiation barrier coatings based on photonic glass macroporous coatings would be superior to that of multistack inverse opals. The maximum wavelength reflected (broadband cutoff) and the absolute values of reflectance can be controlled by varying the microsphere size and by increasing the refractive index contrast. Examples of multistack inverse opals are presented using materials such as TiO_2,[12,18] SiO_2,[13,20] and composites of SiO_2−TiO_2[13] and Al_2O_3−ZnO-TiO_2,[21] none being suitable for high-temperatures applications. The overall reflectance (wavelength range and maximal reflectance) achieved with 2 or 3 stacks of inverse opals with different lattice constants is still not comparable with what can be achieved with photonic glasses.[12,13,18,21] In addition, stacking multiple photonic crystal layers induces losses in the overall reflectance when compared to its single-stack constituents.[17,18,22]

So far, the established techniques to fabricate ceramic photonic glasses consist of depositing a polymeric template followed by infiltration of a ceramic phase using atomic layer deposition (ALD) or chemical vapor deposition (CVD). This approach is extensively used to fabricate inverse photonic crystals despite its limitations.[17,18,23] These infiltration techniques are very time-consuming and have severe limitations for the deposition of ternary compounds, such as yttrium-stabilized zirconia (YSZ), due to the deposition temperature being higher than the glass transition of the polymer template (commonly polystyrene or poly(methyl methacrylate)). YSZ is a material widely used for applications in which a combination of refractory properties, low thermal conductivity, and high hardness are demanded and, due to its high temperature phase stability, is predominantly used for TBCs. As an alternative to such two-step deposition procedures, where deposition of the polymer template and its infiltration by a ceramic phase are performed separately, simultaneous codeposition of the polymer and ceramics in a single step can be carried out. In colloidal systems containing polymer microspheres and alumina[24] or zirconia[25,26] nanoparticles, heterocoagulation was used as a tool to create a polymer−ceramic core−shell spheres. Heterocoagulation results from the mutual attraction of particles carrying the opposite surface charges in suspension. The mixture of large negatively charged polymer spheres and positively charged ceramic nanoparticles induces the formation of a ceramic shell on the surface of the polymer. After drying of the suspension, the polymer template can be removed by calcination, resulting in a structure composed of ceramic shells. However, the optical properties of the macroporous films obtained in this way have never been studied. In the work on zirconia coatings, Jia et al.[25,26] also did not study the relative concentration of ceramic nanoparticles regarding its influence on the layer stability, e.g., shrinkage/cracking.

It should be emphasized that heterocoagulation-based deposition of disordered photonic structures strongly differs from the colloidal coassembly methods reported before.[13,20,27,28] In this case, all particles in the dispersion must bear the surface charges of the same sign to favor the self-assembly process. For the deposition of ordered structures, heterocoagulation needs to be avoided. One advantage of codeposition is that the fabrication of the ceramic phase can be decoupled from the actual fabrication/deposition of the photonic structure. As preparation of the ceramic nanoparticles can be performed separately, other compositions and chemistries are available that could not be achieved otherwise, as in the case of YSZ. Dopants to control other aspects of high-temperature stability can also be readily introduced. Coassembly by heterocoagulation with nanoparticles not only offers simplicity but also allows for the implementation of other chemistries and materials.

In this work, we investigate the feasibility of an all-colloidal and single-step deposition method of YSZ-infiltrated polymeric photonic glass by means of heterocoagulation. A structure formed by a disordered array of monodisperse PS microspheres coated with YSZ nanoparticles was achieved directly by drop-casting the heterocoagulated suspension. After codeposition, annealing was performed to burn-out the polymeric template, resulting in a disordered array of pores of monodisperse size within an interconnected YSZ structure. This straightforward process allowed for the deposition of thin layers exhibiting high reflectance over a broad wavelength range from the visible to near-infrared. Additionally, the effect of the amount of YSZ nanoparticles on the ceramic shell thickness and filling fraction of the structure, which play a large role on the photonic proprieties, was investigated. The thermal stability of these structures was tested up to 1200 °C.

2. EXPERIMENTAL SECTION

As base materials commercial monodispersed PS spheres with a diameter of 756 nm ± 20 nm (Microparticles GmbH), synthesized crystalline YSZ nanoparticles, and deionized water were used. For sake of comparison, monodispersed PS spheres with a diameter of 2.48 μm ± 0.05 μm were also used. Crystalline nanoparticles of YSZ with primary size below 10 nm were produced by a mild hydrothermal synthesis route from corresponding nitrates as described by Guiot et al.[29] Fully stabilized zirconia nanoparticles with the cubic structure were produced by exposing aqueous solutions of zirconyl and yttrium nitrates ($[Zr^{4+}]$ = 0.1 M and $[Y^{3+}]$ = 0.05 M) stabilized by acetylacetone (0.1 M) to a temperature of 160 °C in an autoclave for 3 days. After hydrothermal synthesis, the YSZ stock suspension was purified by dialysis in deionized water using a tubular cellulose membrane. The purified suspension was centrifuged for 1 h at 5000*g* and the supernatant liquid removed. Then the precipitated, concentrated suspension was sonicated for 16 h, resulting in a clear suspension with a concentration of 70 mg mL^{-1} (Ultrasonic processor UP100H, Hielscher Ultrasonics).

Suspensions were prepared in deionized water by mixing stock suspensions of PS spheres with a diameter of 756 nm and YSZ particles. The concentration of PS spheres was maintained constant at 20 mg mL^{-1}, and the concentration of YSZ nanoparticles was varied at 10, 20, 30, 40, and 50 mg mL^{-1}. These concentrations resulted in YSZ/PS ratios of 0.5, 1.0, 1.5, 2.0, and 2.5 by weight. The mixtures were ultrasonicated for 30 min to homogenize the suspension and to promote interaction between polymer and ceramic particles. Suspensions were drop-cast within a silicon ring fixed to a clean, hydrophilic soda-lime silica glass substrate or to a quartz substrate (for high temperature investigations). The substrates were cleaned by soaking in an alkaline detergent solution (Mucasol, Merz Hygiene GmbH) for several hours in an ultrasonic bath, brushing, rinsing subsequently with hot tap water and with deionized water, and blow dried by filtered nitrogen. Due to the fixed silicon ring, the resulting area of the sample was 4.5 cm^2. The amount of suspension deposited was 300 μL for each sample, resulting in thicknesses ranging from 10 to 20 μm depending on the YSZ content. The effect of temperature during deposition was evaluated by heating the substrate on a hot-plate at 40, 70, and 90 °C. As-cast samples were annealed at 500 °C for 30 min in air at a heating rate of 1 °C min^{-1} to eliminate the polymeric

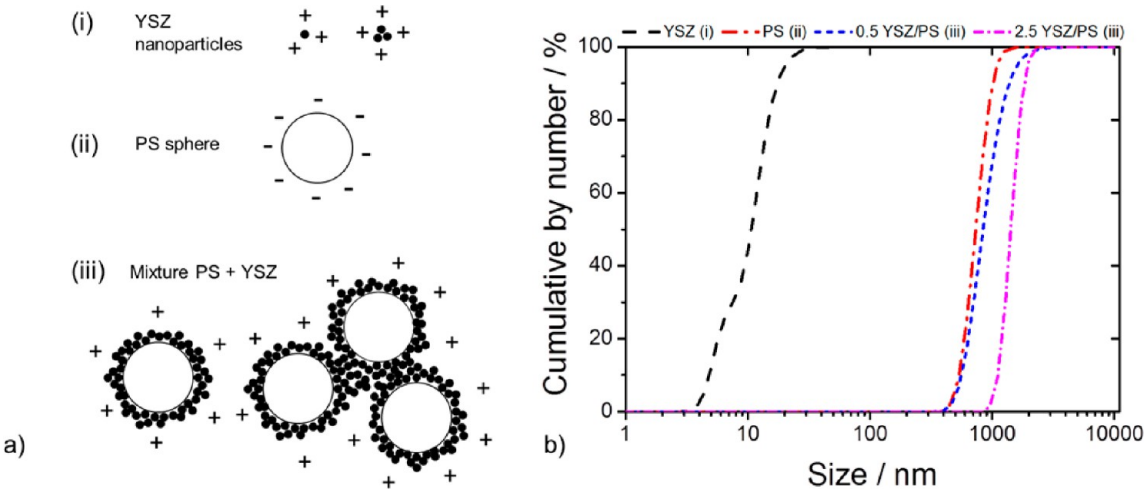

Figure 1. (a) Schematic behavior of particles in suspension and (b) particle size distribution by number measured in diluted suspension from stock suspensions containing only YSZ nanoparticles, only PS particles, and mixtures of 20 mg mL^{-1} of PS particles with 10 mg mL^{-1} (0.5 YSZ/PS) and 50 mg mL^{-1} of YSZ (2.5 YSZ/PS).

template leading to an inverse structure. To increase the overall thickness of the layers, repetitive drop-casting was performed by depositing an additional suspension on top of a preinverted layer. Inverse structures were subsequently annealed at 1000 and 1200 °C for 1 h at a heating rate of 5 °C min^{-1}, analyzed, and then reannealed at the same temperatures for an additional 3 h to investigate their temperature stability.

Particle size distributions and zeta potentials were measured using a Zetasizer Nano S (Malvern Instruments) and a Zetasizer 2000 (Malvern Instruments), respectively. For these two measurements, dilute suspensions were prepared from the stock suspensions of the initial materials and from the suspensions used for drop-casting, according to equipment manufacturer guidelines. The microstructures of the layers and their thickness were observed by a scanning electronic microscope (SEM, Leo 1530 and Zeiss Supra 55 VP, Carl Zeiss). Ordering of spheres in the SEM micrographs was assessed by fast Fourier transform (FFT) implemented in the software ImageJ. X-ray diffraction measurements were performed with Cu−Kα radiation and a GADDS detector (D8 Discover, Bruker AXS). The optical proprieties in the visible and near-infrared spectral regions were measured in diffuse reflectance mode with a spectrometer (Lambda 1050, PerkinElmer) equipped with an integrated sphere setup.

Simulations of the reflectance were performed using the finite-difference time-domain method (FDTD), implemented as a freely available software package Meep,[30] with a resolution of 64 pixels per lattice spacing and subpixel smoothing[31] of the dielectric function for more precise modeling of the finer structural features. The reflectance of visible and infrared electromagnetic radiation in a broad wavelength range was studied. Under normal incidence, the reflectance R depends on the absorption A and the transmission T as follows

$$R = 1 - T - A \tag{1}$$

Due to the very low absorption of YSZ in the visible and NIR range,[32] $A = 0$ is a good approximation. The reflectance was calculated by modeling propagation of a plane wave incident on the disordered structure along the z-axis direction and comparing the intensities of reflected and incident waves. The FDTD calculation region spanned 4.5 μm × 4.5 μm size in the x−y plane, with periodic boundary conditions. Along the z-axis direction, perfectly matched layer boundary conditions were imposed. The thickness of the structure is assumed to comprise 8.5 μm along the z-axis direction. The refractive index of the YSZ is assumed to be $n = 2.12$. The spherical pore size (e.g., pore left by the polymer template) was defined to have a diameter of 756 nm and total volume fraction in the structure of 50%.

The total transmission for a random system with a slab geometry is expressed by photonic Ohm's law which states that the total transmission $T \sim l_t(\lambda)L^{-1}$, where L is the thickness of the sample and $l_t(\lambda)$ is the transport mean free path (the average distance over which the scattered light direction is randomized).[33] The necessary condition for photonic Ohm's law is the transport mean free path $l_t(\lambda) \ll L$ which means that the light has been multiply scattered in the material. An ideal reflector has maximized reflectance in the broad range spectrum for an as small as possible thickness. The following figure of merit function F is proposed

$$F = \frac{1}{T_{av}L} = \frac{1}{(1 - R_{av})L} \tag{2}$$

where

$$T_{av} = \frac{1}{\lambda_2 - \lambda_1}\int_{\lambda_2}^{\lambda_2} T(\lambda)d\lambda \tag{3}$$

is the averaged transmission; $R_{av} = 1 - T_{av}$ is the averaged reflection (for *nonabsorptive materials*); and (λ_1, λ_2) is the wavelength range. Corresponding to photonic Ohm's law, the figure of merit function F is independent of the thickness of the sample. It means F is a function of geometrical parameters of the sample (shape of particle and filling fraction) and the refractive index.

3. RESULTS AND DISCUSSION

3.1. Materials and Suspensions. To gain an understanding of the interaction of heterocoagulation and the formation of core−shell particles in suspension, which allows the facile deposition of disordered arrays of such particles, the zeta potential of these particles was measured. The zeta potentials were determined to be in the ranges of −40 to −50 mV and +40 to +50 mV for the PS microspheres at the as-received pH (~6.5) and the YSZ nanoparticles after dialysis and sonication (pH ~ 5.5), respectively. As the isoelectric point (IEP) of YSZ nanoparticles is at pH ~8 and the PS spheres have no IEP, both colloids are well dispersed. Upon mixing together, the particles heterocoagulated by electrostatic attraction, as the positively charged YSZ nanoparticles are attracted to the negatively charged surface of the PS spheres. Due to the small size of the YSZ nanoparticles compared to the PS spheres, a coating is created on the PS surface leading to a core−shell PS−YSZ particle. Figure 1a schematically depicts the particles (i) in the YSZ stock suspension as single particles or small agglomerates, (ii) in the PS stock suspension a single

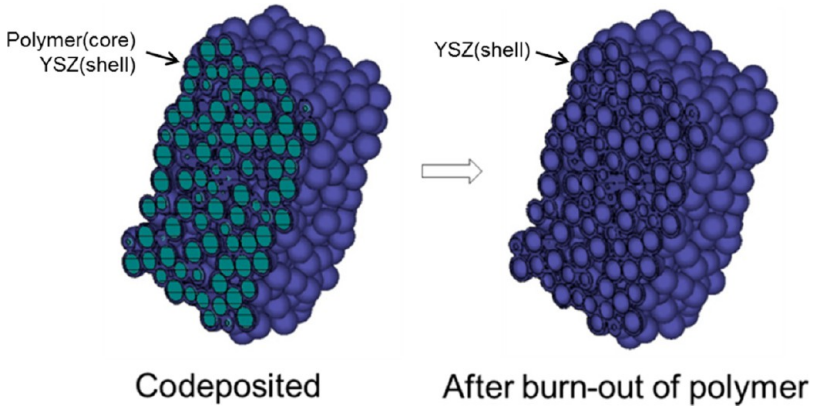

Figure 2. Schematic of a codeposited core-shell structure and a shell-like structure after burn-out of the polymer template.

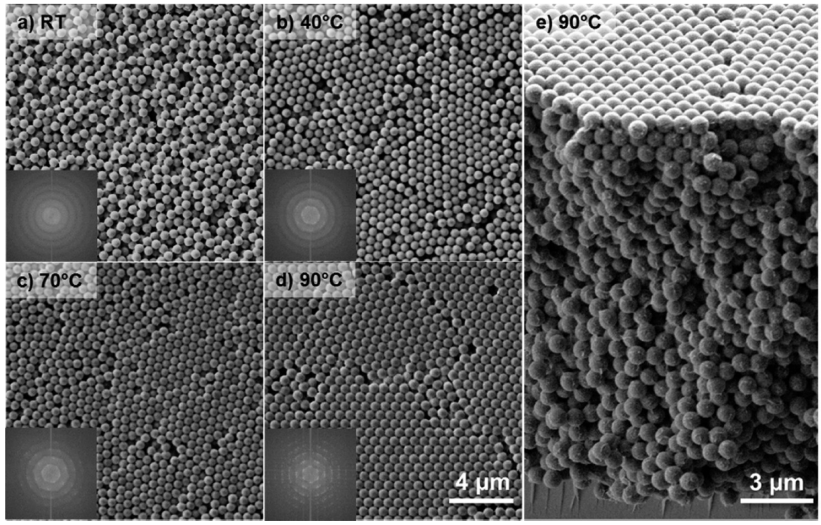

Figure 3. SEM micrographs and corresponding FFT images showing an increase of surface ordering with increasing deposition temperature at (a) room temperature (RT), (b) 40 °C, (c) 70 °C, and (d) 90 °C. FFT analysis confirms the increase ordering in a hexagonal symmetry. (e) Cross-section of a sample deposited at 90 °C showing surface ordering and disordered bulk.

sphere, and (iii) in a mixture of PS and YSZ particles as a single core−shell particle or cluster of core−shell particles.

To determine the behavior of the particles in suspension, particles size analysis was performed. Cumulative particle size distributions are shown in Figure 1b. The particle size distribution of only YSZ nanoparticles shows a bimodal distribution with the first inflection point at 5 nm and second at 12 nm. The first inflection point is related to the primary size of nanoparticles and the second to small agglomerates that have not been broken by sonication. The PS particles present an inflection point at 712 nm with a unimodal distribution consistent with the monodispersity of the PS stock suspension from the supplier. The PS−YSZ mixtures at 0.5 YSZ/PS and 2.5 YSZ/PS also present a unimodal distribution with inflection points at 825 and 1487 nm, respectively. The absence of particles in the YSZ size range for these mixtures indicates that there are no free YSZ nanoparticles in suspension; i.e., all of the nanoparticles are attached to the surface of the PS particles for these ratios of mixture. For the higher YSZ/PS ratio suspension, the increase in particle size after heterocoagulation is larger than expected for one, single-coated PS sphere, which suggests flocculation of coated particles into small clusters up to ∼3 μm in diameter (as depicted in Figure 1b (iii)). Calculated thicknesses considering a YSZ density of 3 g cm^{-3} shell are ∼20 and ∼100 nm for 0.5 YSZ/PS and 2.5 YSZ/PS, respectively. More details on the core−shell heterocoagulated structures will be discussed later in this paper.

The self-assembly of ordered structures is a natural process when dealing with monodisperse spheres such as the PS spheres used in this work. Conversely, this study shows that heterocoagulated particles tend to naturally form disordered structures. The light flocculation promoted by the heterocoagulation appears to be one of the reasons for avoiding self-assembly. Clusters of coated particles are more prone to fast sedimentation and, once deposited, inhibit the self-assembly of other particles. Disorder is further facilitated by favorable particle−substrate interactions,[4,5] e.g., attraction between charged particles and charged substrates during self-assembly. The materials of substrates, soda-lime silica glass, and quartz have their IEP in the pH range of 2−3. In our experiment, the substrates are negatively charged, and the YSZ-coated PS particles are positively charged at the work pH of ∼6. Thus, there is a strong adhesion and low mobility of particles on the substrate due to Coulomb attraction between them, resulting in a disordered structure consistent with the conditions proposed in their work.[4,5]

3.2. Deposition, Microstructure, and Photonic Properties. Figure 2 shows a schematic of a codeposited, core−shell

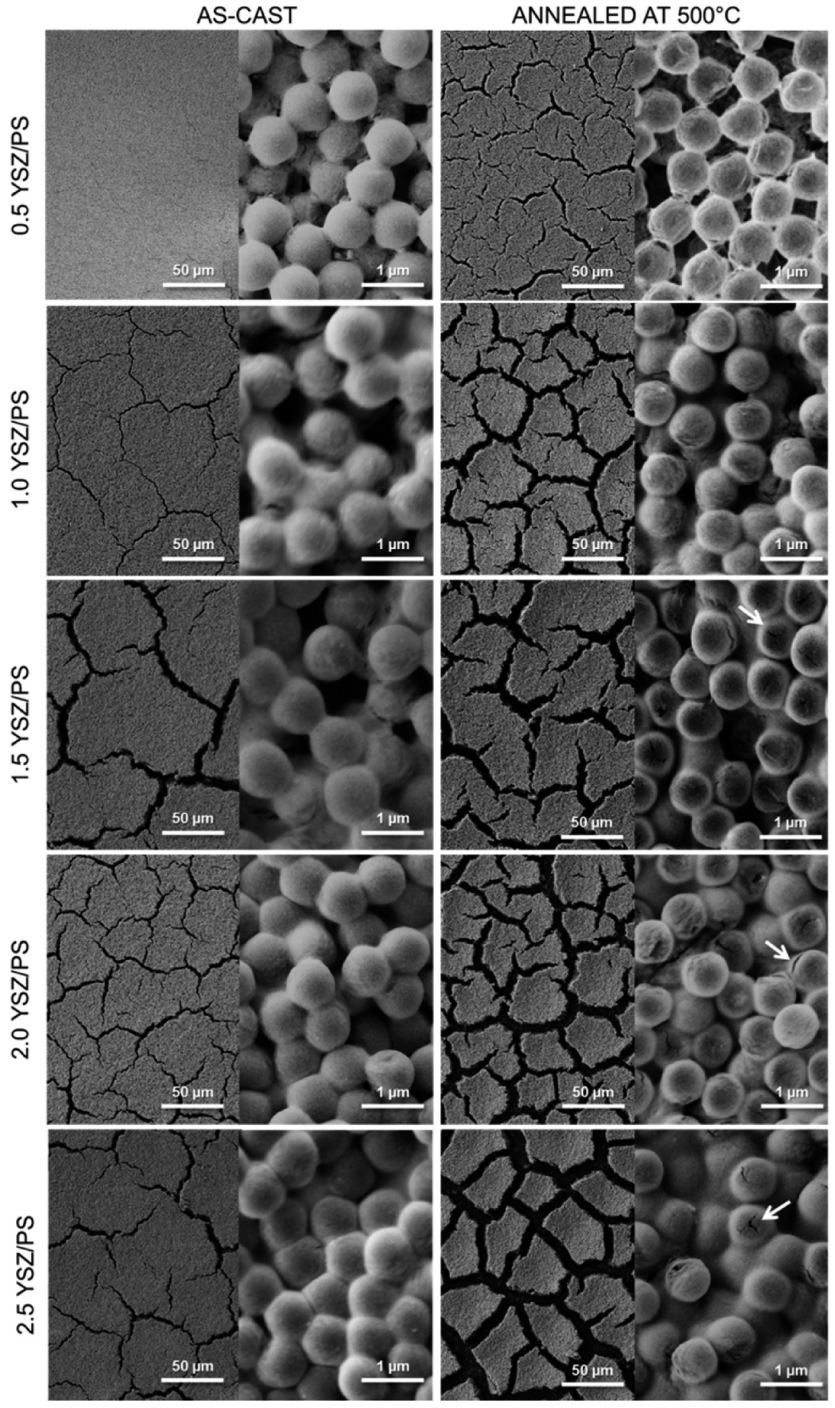

Figure 4. SEM micrographs of as-cast and inverted films with variation of YSZ/PS ratio from 0.5 to 2.5. YSZ/PS ratio was varied by YSZ weight in the precursor suspension. Low and high magnification images are shown for each sample. Arrows show shell cracks due to shrinkage of the shell and/or decomposition gases escaping from the structure during annealing.

structure and the resulting shell-like structure after burn-out of the polymer template. Utilization of nanoparticle codeposition circumnavigates many of the challenges faced by conventional infiltration methods. First, the effect of the deposition temperature on the degree of disorder was explored. A suspension containing 20 mg mL^{-1} of PS spheres and 10 mg mL^{-1} of YSZ nanoparticles (0.5 YSZ/PS) was drop-cast onto glass substrates at various temperatures ranging from room temperature to 90 °C. It was found that the drying time took around 30 s at 90 °C and up to 4 h at room temperature (21 °C). Initial visual inspection of the films suggested an increase in ordering with increasing temperature, as they exhibited a more pronounced (but still weak) green iridescence. The SEM micrographs and corresponding FFT images in Figure 3a–d compare the surface ordering as a function of deposition temperature. With increasing temperature, an increase in ordering can be observed for the top-view microstructures. The FFT analysis confirms this result, showing a shift from a diffuse ring pattern to discrete spots with hexagonal symmetry as the structure shifts from disordered to ordered. As reported by García et al.,[9] an ordered surface structure can hide disordered bulk structures, and for this reason, cross-section

imaging (Figure 3e) in combination with the diffuse reflection can better evaluate the ordering of the entire system. As can be seen in Figure 3e, for the extreme temperature of 90 °C, only a few layers on the top surface are ordered. The diffuse reflection spectra of these as-cast samples did not show any features of an ordered photonic material (i.e., photonic band gap) over the measured wavelengths (Figure S1, see Supporting Information). This suggests that the surface ordering has no considerable influence on the overall diffuse character of the reflectivity. Coatings deposited at different temperatures had very similar reflectance characteristics. However, deposition at room temperature was used in all further experiments to ensure full disorder. The lower limit of the ratio of YSZ/PS that still inhibits self-assembly was not investigated. Nevertheless, the lowest ratio tested (0.5 YSZ/PS) was already enough to fully inhibit self-assembly. This can be seen in the FTT images in Figure 3 for a sample of 0.5 YSZ/PS deposited at room temperature. Lower YSZ/PS ratios were not tested due to the already thin and deformed shells after calcination at 500 °C, as can be observed later in this work. Lower ratios could still inhibit self-assembly but would not result in physically stable structures and therefore would not be practical.

Next, the amount of YSZ nanoparticles in suspension was varied to increase the YSZ-shell thickness in suspension, increasing the total volume of YSZ in the structure. Figure 4 compares as-cast and inverse samples varying the YSZ concentrations in suspension. The creation of a core−shell prior deposition (in suspension) is important to ensure homogeneity of the deposited structure. Free nanoparticles in these systems result in electrostatic attraction of these positively charged nanoparticles to the negatively charged substrate as can be seen in Figure S2 (see Supporting Information) in a comparison using suspension with 2.5 YSZ/PS ratio using different PS sizes (756 nm and 2.48 μm). It is assumed that the lower surface area of the larger PS particles is the reason for a lower amount of nanoparticles heterocoagulated. Assuring complete heterocoagulation, a homogeneous photonic glass layer can be obtained.

The concentration of YSZ nanoparticles influences the shell thickness and the filling fraction of the spaces between the PS particles and thereby influences the stability of the structure to cracking and distortion of pores. On annealed layers (Figure 4, second column), with the increase of YSZ content from 0.5 to 1.0 YSZ/PS, the shells present a significant increase on diameter from ∼700 to ∼735 nm. For higher concentrations, the increase in diameter was much less pronounced, measured to be up to ∼750 nm for 2.5 YSZ/PS. The stagnation of shell diameter after deposition supports the hypotheses of increasing the ceramic filling fraction between the deposited PS particles (transitions from a shell-like to a filled structure), which can also be observed on the SEM images. At the lowest YSZ concentration, the shell is slightly deformed due to the thin shell thickness. For higher concentrations, the resulting shell maintains its shape, but small cracks in the shell can be observed. These cracks can be the result of shrinkage of the shell and/or polymer decomposition gases escaping from the structure during annealing. The increase in the amount of YSZ nanoparticles also has a detrimental effect on the total area of large cracks in the films, as shown in Figure 5. At the lowest concentration of nanoparticles the area fraction of cracks is around 1%, but it is increased up to 35% at the highest concentration tested. These cracks are present due to the shrinkage of the ceramic phase (i.e., increase of packing density

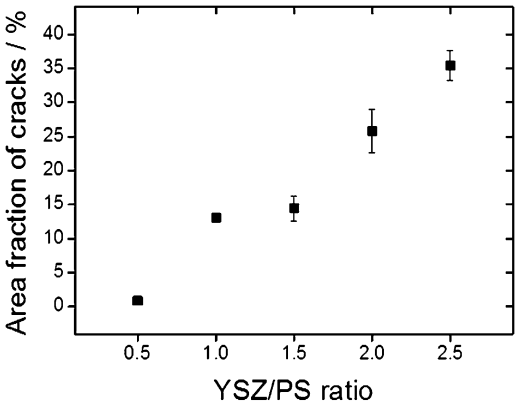

Figure 5. Area fraction of cracks (%) of films with standard deviation in films after inversion as a function of YSZ/PS ratio in suspension.

of nanoparticles) induced by the drying process in the as-cast samples, and the effect becomes more pronounced after annealing at 500 °C.

After decomposition of the polymer by annealing at 500 °C for 30 min, the diffuse reflectance of the photonic glass samples as a function of the YSZ content was measured (Figure 6a). The inverse structures show broadband diffuse scattering, as expected for photonic glasses. The maximum values of reflectance are on the order of 50% over a broad wavelength range of 0.4−2.0 μm for photonic glasses with YSZ/PS ratios of 2.0 and 2.5. The simulations (Figure 6b) evaluate the increase of shell thickness (from 60 to 300 nm) and the increase of

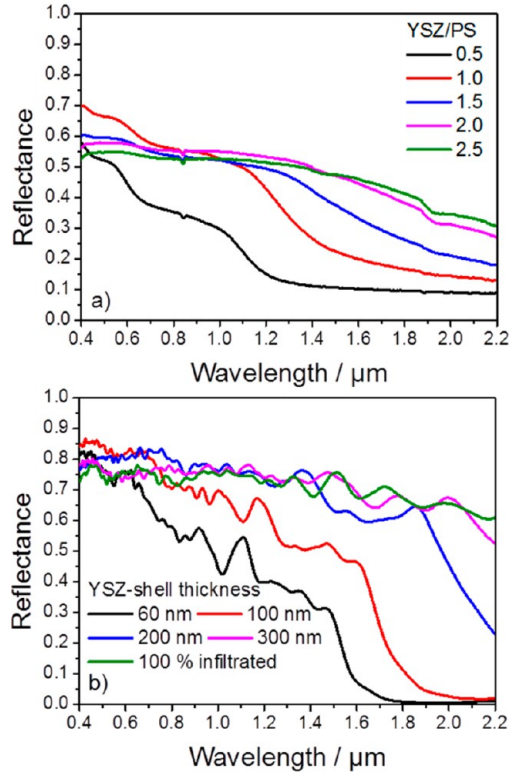

Figure 6. (a) Experimental reflectance spectra of YSZ inverse photonic glasses as a function of YSZ concentration (YSZ/PS weight ratio in the suspension) and (b) simulations performed for YSZ inverse photonic glasses with various shell thicknesses and for a fully infiltrated structure.

filling fraction (by comparing thin shells with a completely filled structure). With the increase of YSZ content two consequences can be observed: (i) the cutoff of the high-reflectance band shifts to longer wavelengths and (ii) the overall reflectance increases. Both effects have been shown to be strongly dependent on YSZ content, due to an increase of material volume of high refractive index (compared with air of pores). These trends are observed both in simulations as well as in the measurements. Increasing the amount of high reflective index (the YSZ) either by increasing shell thickness or filling fraction of the structure can be used to improve the reflectance of photonic glasses.

Figure 7 compares the diffuse reflection spectrum of a photonic glass from this work (YSZ/PS 2.5) to the specular

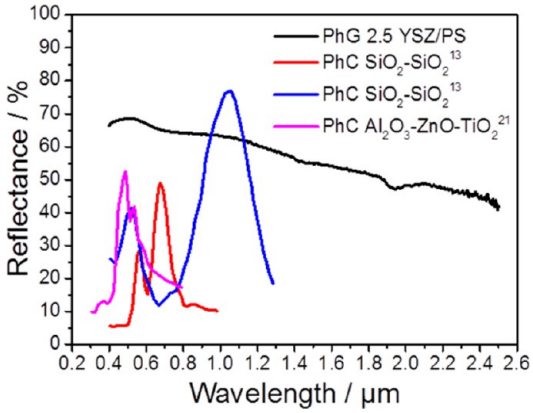

Figure 7. Comparison of the diffuse reflection spectrum of a photonic glass from this work (PhG 2.5 YSZ/PS) with specular reflection spectra multistack photonic crystals (PhCs). In red double-stack SiO_2−SiO_2[13] with pore sizes of 560 and 435 nm, in blue with pore sizes of 715 and 420 nm, and in magenta a triple-stack composite of Al_2O_3−ZnO−TiO_2[13] with a single pore size of 270 nm.

reflection spectra of multistack inverse photonic crystals from the literature. Multistack inverse crystal using materials such as SiO_2[13] and composites of Al_2O_3−ZnO−TiO_2[21] achieved maxima in the range of 30−80% and 30−55%, respectively. However, everywhere outside the photonic bandgap, the reflectance of photonic crystals is substantially lower. Not only is the maximum intensity from the photonic glass comparable with double- and triple-stack photonic crystals but also its intensity is maintained over a larger wavelength range. The reflection spectra of double- and triple-stack photonic crystals are better described as multipeak than as broadband. In addition, comparing photonic glasses and photonic crystals fabricated from YSZ nanoparticles, the achieved reflectance for a single-layer photonic glass is 2 to 5 times more intense compared to a single-stack photonic crystal.[27]

It is important to highlight that even with crack areas as high as 35% for samples with the highest YSZ content, reflectance up to 55% for wavelengths around 0.5 μm and 40% for wavelengths of 2 μm was achieved. However, the reflectance could be improved by increasing the film thickness and optimizing the process to decrease the crack density. Therefore, a multiple layer approach was performed aiming (i) to increase the overall thickness of the film and (ii) to fill in the cracks in the previous layers. During the process, the cracks in the previous layer are filled with some of the suspension from the deposition of the subsequent layer. These two processes work together to improve the overall reflectance. The SEM micrograph in Figure 8 shows a double-layer sample post

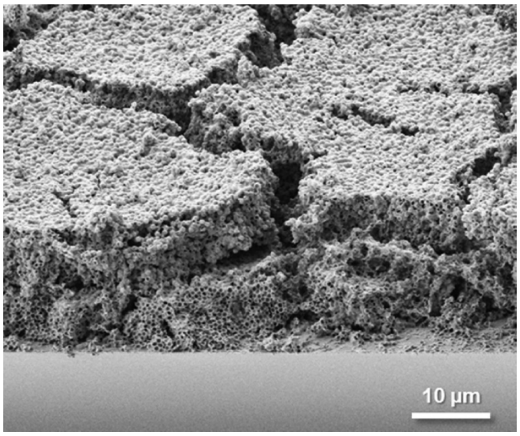

Figure 8. Cross-sectional SEM micrograph of a double-layer sample deposited from suspension 1.5 YSZ/PS in weight after burn-out of the polymer template.

burn-out (1.5 YSZ/PS). Cracks in the first layer were successfully filled. The reflectance behavior of samples deposited from suspensions 0.5 YSZ/PS, 1.5 YSZ/PS, and 2.5 YSZ/PS up to three layers thick is shown in Figures 9a, b, and c, respectively. It was not possible to achieve meaningful measurements for the third layer from the suspension 2.5 YSZ/PS due to problems with the adhesion of the film on the substrate. The results demonstrate multiple-layer deposition as a promising and simple method to mitigate the effect of cracking and improve the overall reflectance. The best results were achieved with the deposition of three layers from the suspension 1.5 YSZ/PS, which demonstrated ∼80% reflectance over the visible and near-infrared region of the spectra (0.4−1.4 μm).

Figure 9d shows the integrated reflectance over the measured wavelength range (0.4−2.2 μm) as a function of total film thickness (related to the number of layers). Up to 70% integrated reflectance was archived for layers from suspensions 1.5 YSZ/PS and 2.5 YSZ/PS with thicknesses within 30−40 μm. The error bars represent the measurement over the length of the sample cross-section, with a standard deviation up to ∼15%. For the case of one layer deposited from suspension 2.5 YSZ/PS with thickness of ∼16 μm, this equates to a thickness difference of about only three sphere sizes over the entire 2.5 cm length of the sample. As such, relatively uniform films were achieved.

The figure of merit function F, representing the reflectance efficiency of the layers, for the measured wavelength range (0.4−2.2 μm) for samples 0.5 YSZ/PS, 1.5 YSZ/PS, and 2.5 YSZ/PS was determined to be 0.0200 μm^{-1}, 0.0627 μm^{-1}, and 0.0570 μm^{-1}, respectively. The YSZ-inverse photonic glass films demonstrated in this work potentially would be able to achieve 93% reflectance for the wavelength range at a thickness of 220 μm (F = 0.0627 μm^{-1}) for the 1.5 YSZ/PS samples.

TBCs are commonly deposited by air plasma spraying (APS) or by electron beam physical vapor deposition (EBPVD).[34] Both methods, APS[35] and EBPVD,[36] are a focus of reflectance optimization. APS allows for the modification of the microstructure with features like pores and microcracks in the deposited TBCs aiming to improve its scattering properties. For comparison, to obtain the same efficiency (93% reflectance,

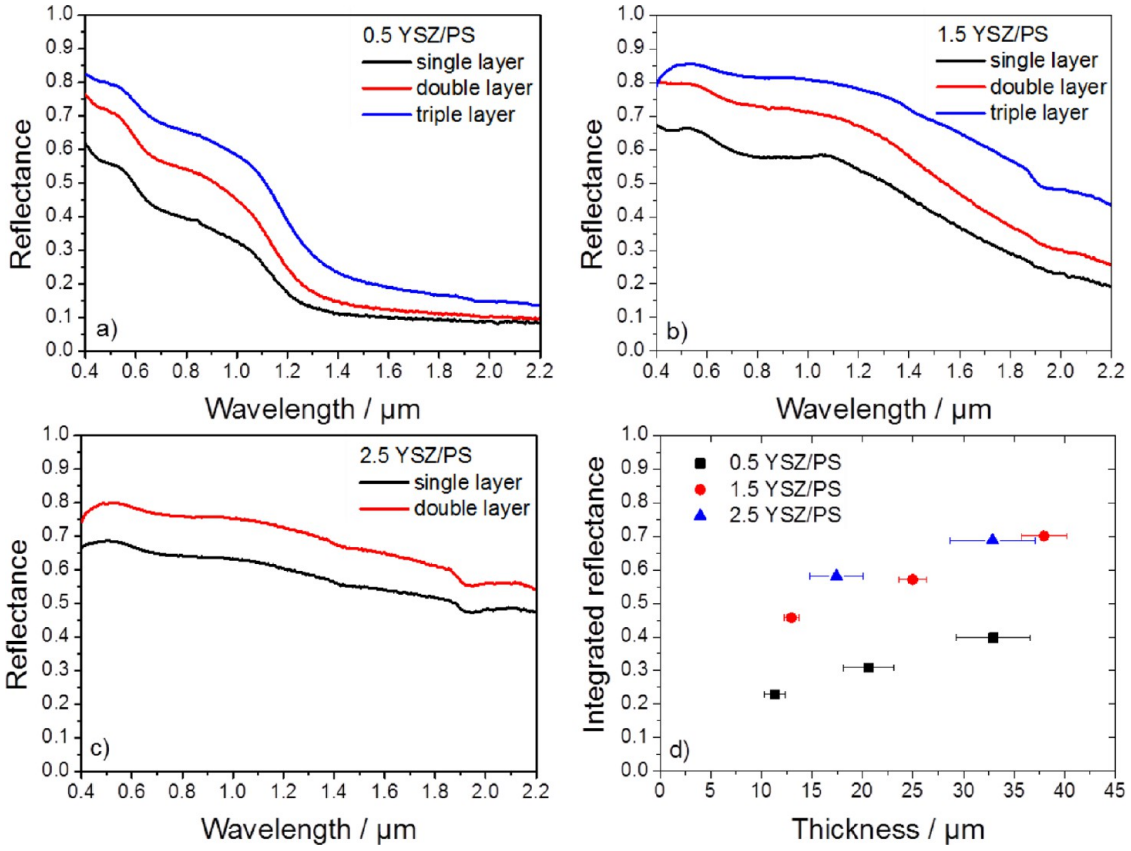

Figure 9. Reflectance spectra as a function of the number of layers for films deposited from suspensions (a) 0.5 YSZ/PS, (b) 1.5 YSZ/PS, and (c) 2.5 YSZ/PS. (d) Integrated reflectance over the measured wavelength range (0.4–2.2 μm) as a function of the total film thickness and YSZ/PS ratio.

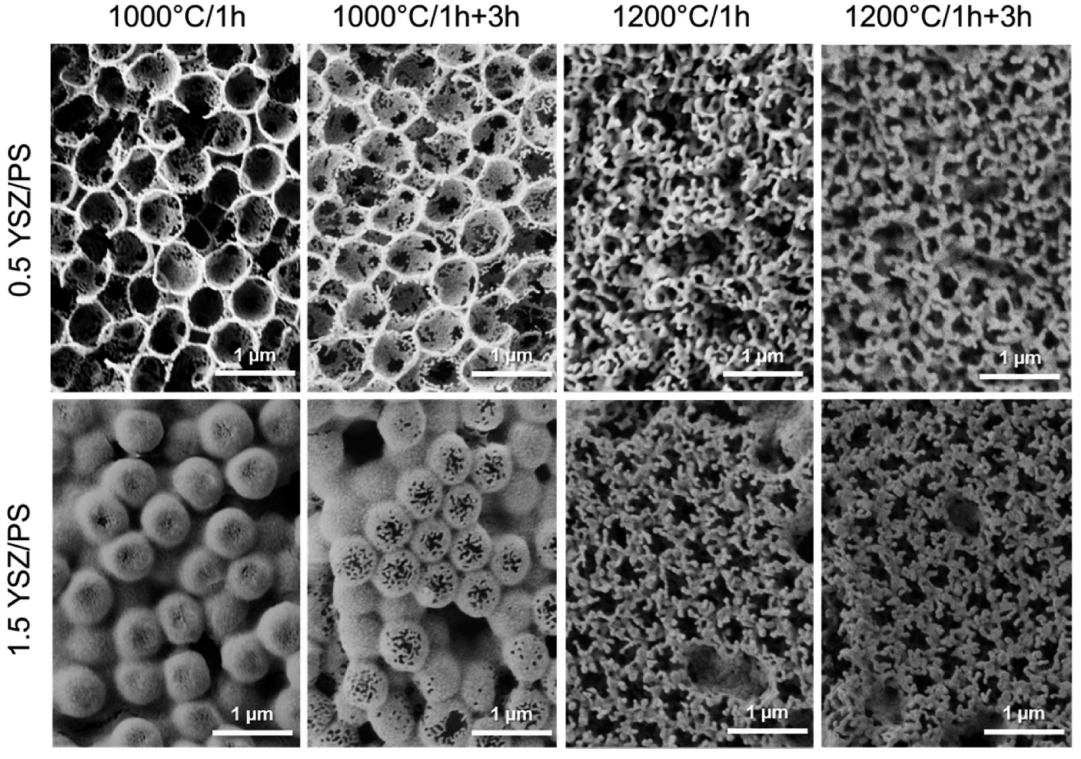

Figure 10. SEM micrographs of films deposited from suspension 0.5 YSZ/PS and 1.5 YSZ/PS after annealing at 1000 and 1200 °C for 1 h and subsequently for additional 3 h.

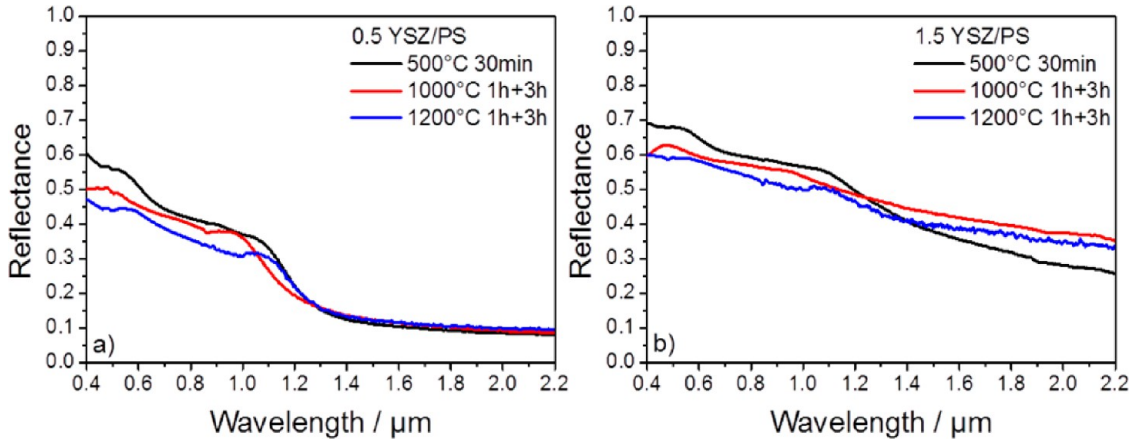

Figure 11. Experimental reflectance spectra as a function of annealing temperature and time for films deposited from suspensions (a) 0.5 YSZ/PS and (b) 1.5 YSZ/PS. The case of 30 min at 500 °C represents the removal of the PS polymer spheres via calcination only (inversion).

220 μm thick layer) as the photonic glass deposited from the suspension 1.5 YSZ/PS, a 370 μm thick layer by plasma-sprayed YSZ deliberately optimized for high diffuse reflectance would be needed.[35] Therefore, the inverse photonic glass films can offer an advantage of achieving similar values of reflectance using the films about 40% thinner than those produced by other advanced TBC deposition methods.

3.3. High-Temperature Behavior. To evaluate the high-temperature behavior, two different layers were chosen. Layers deposited from suspensions 0.5 YSZ/PS and 1.5 YSZ/PS were tested due to their different structure (i.e., YSZ content). Figure 10 shows samples with two different shell thicknesses annealed at 1000 and 1200 °C for 1 h and subsequently at the same temperatures for an additional 3 h. Samples with thinner shells (0.5 YSZ/PS) exhibited more pronounced structure degradation when compared to thicker shells (1.5 YSZ/PS). While shrinkage and grain growth are observed with an increase in temperature and time, the pore structure is maintained without losing its spherical form at 1000 °C. At 1200 °C the initial shape is still discernible for the thicker shells; however, the thinner shells have completely lost their spherical shell shape, but porosity is still observed. Due to these structural changes there is a decrease of the reflection level (Figure 11); however, reflection is still high because the structure is strongly optically inhomogeneous, and the spherical pores still define the scattering properties. In addition to structural stability, the phase stability with temperature was examined. XRD spectra of the initial nanoparticles and films (Figure 12) are consistent with the cubic phase of fully stabilized, yttrium-doped zirconia (JCPDS 30-1468). The cubic phase of the as-synthesized nanoparticles is maintained after burn-out at 500 °C and after several hours at 1000 and 1200 °C. At elevated temperature, narrowing of the peaks is observed, indicating significant grain growth.

The high structural and optical stability of the macroporous YSZ coatings should enable utilization of photonic broadband reflectors at high temperatures. To obtain a refractory coating which could reflect the thermal radiation in the range 1−5 μm relevant for TBC applications,[17] the described approach should be modified for pores with larger inner diameter, i.e., using polymeric particles of correspondingly larger size.

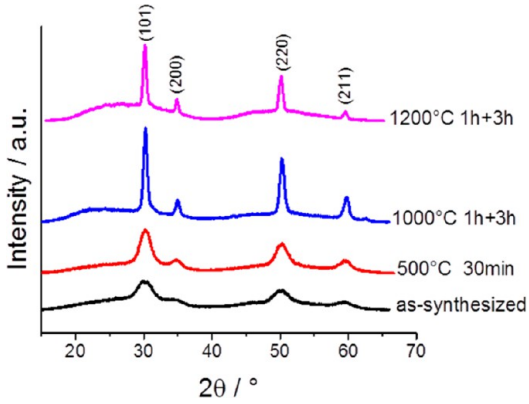

Figure 12. XRD spectra of as-synthesized YSZ nanoparticles, after inversion at 500 °C for 30 min, at 1000 °C, and at 1200 °C for 1h + 3h. Cubic structure of fully stabilized, yttrium-doped zirconium oxide indexed (JCPDS 30-1468).

4. CONCLUSIONS

We presented an alternative, all-colloidal, and single-step deposition method of YSZ-inverse photonic glass films. Self-assembly of ordered colloidal crystals can be avoided by promoting heterocoagulation in a suspension containing negatively charged PS spheres and positively charged YSZ nanoparticles. Colloidal stability of the dispersion is suppressed in this case, so that PS/YSZ core−shell particles flocculate and arrange themselves randomly. After burn-out of the polymer template, the structure is composed of a disordered array of YSZ shells. The YSZ/PS ratio was varied, and its influence (increase of shell thickness and filling fraction) has shown a positive influence on the reflection behavior. The 35 μm thick photonic glasses exhibited high reflectance over a broad wavelength range from the visible to near-infrared. By depositing multiple layers, thicker layers were produced and the effect of cracking minimized to achieve higher overall reflectance. Integrated reflectance of approximately 70% was obtained in the wavelengths range of 0.4−2.2 μm. The high-temperature stability of the YSZ structure (tested up to 1200 °C) is promising for the future applications of photonic glasses where refractory photonic materials are required. The proposed deposition method could also be used with nanoparticles of other ceramic materials. The presented photonic glasses have a much better broadband reflectance when compared with

double- or triple-layer stacks of photonic crystals being very suitable for photonic broadband reflectors.

■ ASSOCIATED CONTENT

Supporting Information

Figure S1: Diffuse reflection spectra of as-cast samples deposited at various temperatures. Figure S2: Layers deposited from suspensions 2.5 YSZ/PS using different PS sphere diameters of 756 nm and 2.48 μm. This material is available free of charge via the Internet at http://pubs.acs.org.

■ AUTHOR INFORMATION

Corresponding Author

*E-mail: g.schneider@tuhh.de.

Author Contributions

The manuscript was written through contributions of all authors. All authors have given approval to the final version of the manuscript.

Notes

The authors declare no competing financial interest.

■ ACKNOWLEDGMENTS

The authors gratefully acknowledge financial support from the German Research Foundation (DFG) via SFB 986 "Tailor-Made Multi-Scale Materials Systems: M^3", projects C2, C4, and C5. We also would like to thank Sweety Mohanty and Prof. Irina Smirnova for the support in hydrothermal synthesis of YSZ nanoparticles.

■ ABBREVIATIONS

YSZ, yttrium-stabilized zirconia; PS, polystyrene; TBC, thermal barrier coating; ALD, atomic layer deposition; CVD, chemical vapor deposition; FFT, fast Fourier transform; FDTD, finite-difference time-domain (simulation method); IEP, isoelectric point

■ REFERENCES

(1) Shi, L.; Zhang, Y.; Dong, B.; Zhan, T.; Liu, X.; Zi, J. Amorphous Photonic Crystals with Only Short-Range Order. *Adv. Mater.* **2013**, *25*, 5314−5320.

(2) Wiersma, D. S. Disordered Photonics. *Nat. Photonics* **2013**, *7*, 188−196.

(3) García, P. D.; Sapienza, R.; Blanco, Á.; López, C. Photonic Glass: A Novel Random Material for Light. *Adv. Mater.* **2007**, *19*, 2597−2602.

(4) Yan, Q.; Gao, L.; Sharma, V.; Chiang, Y.-M.; Wong, C. C. Particle and Substrate Charge Effects on Colloidal Self-Assembly in a Sessile Drop. *Langmuir* **2008**, *24*, 11518−11522.

(5) Tan, K. W.; Koh, Y. K.; Chiang, Y.-M.; Wong, C. C. Particulate Mobility in Vertical Deposition of Attractive Monolayer Colloidal Crystals. *Langmuir* **2010**, *26*, 7093−7100.

(6) Li, H.-L.; Marlow, F. Solvent Effects in Colloidal Crystal Deposition. *Chem. Mater.* **2006**, *18*, 1803−1810.

(7) Cai, Z.; Teng, J.; Yan, Q.; Zhao, X. Solvent Effect on the Self-Assembly of Colloidal Microspheres via a Horizontal Deposition Method. *Colloids Surf., A* **2012**, *402*, 37−44.

(8) Emoto, A.; Fukuda, T. Tailored Assembly of Colloidal Particles: Alternative Fabrication of Photonic Crystal or Photonic Glass. *Appl. Phys. Lett.* **2012**, *100*, 131901.

(9) García, P. D.; Sapienza, R.; López, C. Photonic Glasses: A Step Beyond White Paint. *Adv. Mater.* **2010**, *22*, 12−19.

(10) Gottardo, S.; Sapienza, R.; García, P. D.; Blanco, A.; Wiersma, D. S.; López, C. Resonance-Driven Random Lasing. *Nat. Photonics* **2008**, *2*, 429−432.

(11) Halaoui, L. I.; Abrams, N. M.; Mallouk, T. E. Increasing the Conversion Efficiency of Dye-Sensitized TiO 2 Photoelectrochemical Cells by Coupling to Photonic Crystals. *J. Phys. Chem. B* **2005**, *109*, 6334−6342.

(12) Yan, Q.; Teh, L. K.; Shao, Q.; Wong, C. C.; Chiang, Y.-M. Layer Transfer Approach to Opaline Hetero Photonic Crystals. *Langmuir* **2008**, *24*, 1796−1800.

(13) Cai, Z.; Liu, Y. J.; Teng, J.; Lu, X. Fabrication of Large Domain Crack-Free Colloidal Crystal Heterostructures with Superposition Bandgaps Using Hydrophobic Polystyrene Spheres. *ACS Appl. Mater. Interfaces* **2012**, *4*, 5562−5569.

(14) Chen, K. M.; Sparks, A. W.; Luan, H.-C; Lim, D. R.; Wada, K.; Kimerling, L. C. SiO2/TiO2 Omnidirectional Reflector and Microcavity Resonator via the Sol-Gel Method. *Appl. Phys. Lett.* **1999**, *75*, 3805.

(15) Leontyev, V.; Hawkeye, M.; Kovalenko, A.; Brett, M. J. Omnidirectional Reflection from Nanocolumnar TiO2 Films. *J. Appl. Phys.* **2012**, *112*, 84317.

(16) Ariza-Flores, A. D.; Gaggero-Sager, L. M.; Agarwal, V. White Metal-Like Omnidirectional Mirror from Porous Silicon Dielectric Multilayers. *Appl. Phys. Lett.* **2012**, *101*, 31119.

(17) Lee, H. S.; Kubrin, R.; Zierold, R.; Petrov, A. Yu.; Nielsch, K.; Schneider, G. A.; Eich, M. Thermal Radiation Transmission and Reflection Properties of Ceramic 3D Photonic Crystals. *J. Opt. Soc. Am. B* **2012**, *29*, 450−457.

(18) Kubrin, R.; Lee, H. S.; Zierold, R.; Petrov, A. Yu.; Janssen, R.; Nielsch, K.; Eich, M.; Schneider, G. A. Stacking of Ceramic Inverse Opals with Different Lattice Constants. *J. Am. Ceram. Soc.* **2012**, *95*, 2226−2235.

(19) Shklover, V.; Braginsky, L.; Witz, G.; Mishrikey, M.; Hafner, C. High-Temperature Photonic Structures. Thermal Barrier Coatings, Infrared Sources and Other Applications. *J. Comput. Theor. Nanosci.* **2008**, *5*, 862−893.

(20) Hatton, B.; Mishchenko, L.; Davis, S.; Sandhage, K. H.; Aizenberg, J. Assembly of Large-Area, Highly Ordered, Crack-Free Inverse Opal Films. *Proc. Natl. Acad. Sci. U.S.A.* **2010**, *107*, 10354−10359.

(21) Hwang, D.-K; Noh, H.; Cao, H.; Chang, R. P. H. Photonic Bandgap Engineering with Inverse Opal Multistacks of Different Refractive Index Contrasts. *Appl. Phys. Lett.* **2009**, *95*, 91101.

(22) Koenderink, A.; Lagendijk, A.; Vos, W. Optical Extinction Due to Intrinsic Structural Variations of Photonic Crystals. *Phys. Rev. B* **2005**, *72*, 153102.

(23) King, J. S.; Graugnard, E.; Summers, C. J. TiO2 Inverse Opals Fabricated Using Low-Temperature Atomic Layer Deposition. *Adv. Mater.* **2005**, *17*, 1010−1013.

(24) Tang, F.; Fudouzi, H.; Sakka, Y. Fabrication of Macroporous Alumina with Tailored Porosity. *J. Am. Ceram. Soc.* **2003**, *86*, 2050−2054.

(25) Jia, Y.; Duran, C.; Hotta, Y.; Sato, K.; Watari, K. Macroporous ZrO2 Ceramics Prepared from Colloidally Stable Nanoparticles Building Blocks and Organic Templates. *J. Colloid Interface Sci.* **2005**, *291*, 292−295.

(26) Jia, Y.; Duran, C.; Hotta, Y.; Sato, K.; Watari, K. The Effect of Polyelectrolyte on Fabrication of Macroporous ZrO2 Ceramics. *J. Mater. Sci.* **2005**, *40*, 2903−2909.

(27) Kubrin, R.; do Rosario, J. J.; Lee, H. S.; Mohanty, S.; Subrahmanyam, R. P.; Smirnova, I.; Petrov, A.; Petrov, A. Yu.; Eich, M.; Schneider, G. A. Vertical Convective Coassembly of Refractory YSZ Inverse Opals from Crystalline Nanoparticles. *ACS Appl. Mater. Interfaces* **2013**, *5*, 13146−13152.

(28) Seo, Y. G.; Woo, K.; Kim, J.; Lee, H.; Lee, W. Rapid Fabrication of an Inverse Opal TiO2 Photoelectrode for DSSC Using a Binary Mixture of TiO2 Nanoparticles and Polymer Microspheres. *Adv. Funct. Mater.* **2011**, *21*, 3094−3103.

(29) Guiot, C.; Grandjean, S.; Lemonnier, S.; Jolivet, J.-P.; Batail, P. Nano Single Crystals of Yttria-Stabilized Zirconia. *Cryst. Growth Des.* **2009**, *9*, 3548−3550.

(30) Oskooi, A. F.; Roundy, D.; Ibanescu, M.; Bermel, P.; Joannopoulos, J. D.; Johnson, S. G. Meep: A Flexible Free-Software Package for Electromagnetic Simulations by the FDTD Method. *Comput. Phys. Commun.* **2010**, *181*, 687−702.
(31) Farjadpour, A.; Roundy, D.; Rodriguez, A.; Ibanescu, M.; Bermel, P.; Joannopoulos, J. D.; Johnson, S. G.; Burr, G. W. Improving Accuracy by Subpixel Smoothing in the Finite-Difference Time Domain. *Opt. Lett.* **2006**, *31*, 2972−2974.
(32) Wang, D.; Huang, X.; Patnaik, P. Design and Modeling of Multiple Layered TBC System with High Reflectance. *J. Mater. Sci.* **2006**, *41*, 6245−6255.
(33) Garcia, N.; Genack, A. Z.; Lisyansky, A. A. Measurement of the Transport Mean Free Path of Diffusing Photons. *Phys. Rev. B* **1992**, *46*, 14475−14479.
(34) Clarke, D. R.; Oechsner, M.; Padture, N. P. Thermal-barrier Coatings for More Efficient Gas-Turbine Engines. *MRS Bull.* **2012**, *37*, 891−898.
(35) Stuke, A.; Kassner, H.; Marqués, J.-L; Vassen, R.; Stöver, D.; Carius, R. Suspension and Air Plasma-Sprayed Ceramic Thermal Barrier Coatings with High Infrared Reflectance. *Int. J. Appl. Ceram. Technol.* **2012**, *9*, 561−574.
(36) Wolfe, D. E.; Singh, J.; Miller, R. A.; Eldridge, J. I.; Zhu, D.-M. Tailored Microstructure of EB-PVD 8YSZ Thermal Barrier Coatings With Low Thermal Conductivity and High Thermal Reflectivity for Turbine Applications. *Surf. Coat. Technol.* **2005**, *190*, 132−149.